COMMUNICATION

Check for updates

From brew to clean fuel: harnessing distillery wastewater for electrolysis H₂ generation using nano scale nickle selenide water oxidation catalysts†

Michael Walsh,[a] Jeannie Z. Y. Tan, [ID] [a] Sanjay Nagarajan,[b] Kenneth Macgregor,[c] John M. Andresen,[a] M. Mercedes Maroto-Valer [ID] [a] and Sudhagar Pitchaimuthu [ID] *[a]

This study reports a promising and innovative approach for electrochemical green H₂ generation using distillery industry wastewater. We employed solvothermally derived Ni₂Se₃ nanoparticles with a particle size of ~50 nm as the anode catalyst material to effectively oxidise the acetic acid present in the distillery wastewater. The utilisation of a Ni₂Se₃ nanoparticle-coated stainless steel electrode significantly enhanced the current density (282 mA cm⁻²) in the electrochemical cell compared to the pristine SS (stainless steel) electrode (146 mA cm⁻²) at 2 V RHE. Also, the distillery wastewater electrolyte based cell exhibits higher current density compared to conventional freshwater (*i.e.*, NaOH-based) electrolyte. The distillery wastewater electrolyte demonstrated remarkable H₂ gas evolution (~15 mL h⁻¹ cm⁻²), showcasing its potential for sustainable H₂ generation. However, it was observed that the aggressive bubbling effect at the cathode led to a lower H₂ evolution reaction activity when compared to the freshwater-based electrolyte, which displayed a H₂ production rate of ~22 mL h⁻¹ cm⁻². These findings underscore the potential of employing Ni₂Se₃ as an effective oxidation catalyst in the production of H₂ gas from pre-treated brewery wastewater H₂ gas. The utilisation of Ni₂Se₃ nanoscale water oxidation catalysts in this context opens up new possibilities for both wastewater treatment and H₂ production, paving the way for a more sustainable and resource-efficient future.

1 Introduction

With the world's population ever increasing, and in turn a constant growth of industrial activity and modernisation, the demand for energy across the globe has never been higher. This increase in demand for energy can be seen in the rise of greenhouse gas emissions as more hydrocarbons are consumed in order to meet the worlds energy needs.[1] The overuse of natural hydrocarbon resources causes significant harm to Earth's ecosystem and climate.[2] Consequently, affordable sustainable energy access is crucial for survival. Scientific knowledge has positively impacted key advancements in this area and has been crucial in the development of green H₂ technology. Primarily, increasing interest in electrocatalytic H₂ generation as a greener alternative to carbon-emitting processes, such as steam methane reforming, is becoming more evident.[3–5]

In the electrochemical method, 9 kg of water is required to produce 1 kg of H₂.[6] With regards to the global target of net-zero emissions, the availability of sustainable H₂ is key to achieving these aims. This is evident in the goal of ~15 Mt green H₂ generation by 2030. In this context, it becomes clear that a significant amount of freshwater will be required.[7] Currently, ~20.5 billion litres of freshwater are consumed annually in the electrolysis process for H₂ production. However, it is important to note that this accounts for only 1.5 parts per million (ppm) of the Earth's available freshwater. When compared to sectors like irrigated agriculture, which utilise over 2700 billion cubic meters of water each year, the water requirement for H₂ production remains relatively minimal.[8] Despite its low impact on the overall water supply chain, concerns about freshwater scarcity necessitate a reduction in water extractions from all available sources. Therefore, it becomes crucial to explore solutions that enable H₂ production to utilise the abundant wastewater resources available on Earth. By tapping into wastewater resources, the water footprint of H₂ can be further reduced, alleviating pressure on the freshwater supply chain and promoting sustainability.

Recent studies had examined the potential of using industrial wastewater as a raw material for photo- and electrocatalytic H₂ generation.[9–13] This promising development suggested that industrial wastewater could be a viable alternative to freshwater resources. One approach involved identifying regional

[a]Research Centre for Carbon Solutions (RCCS), Institute of Mechanical, Processing and Energy Engineering, School of Engineering and Physical Sciences, Heriot-Watt University, UK. E-mail: S.Pitchaimuthu@hw.ac.uk

[b]Department of Chemical Engineering, University of Bath, Bath BA27AY, UK

[c]The Scotch Whisky Research Institute, The Robertson Trust Building, Research Avenue North, Riccarton, Edinburgh, EH14 4AP, UK

† Electronic supplementary information (ESI) available: Details of SEM, CV, NMR, results. See DOI: https://doi.org/10.1039/d3se01445b

wastewater sources, such as the wastewater produced from Scotch whisky production, which is currently discharged into local rivers after physical or chemical treatment processes. However, resource recovery from this wastewater stream is crucial. By implementing systems for recovery, treatment, and reuse, a significant portion of the wastewater can be repurposed for activities, such as boiler feed water and cooling processes, leading to reduced disposal costs.[14,15] Depending on the composition of the brewery wastewater, the presence of sugars, alcohol, and soluble starch allow the wastewater to be utilised for biogas production. However, there is still considerable potential for utilising this wastewater in the electrolysis process due to its high biomass content.[16,17]

In recent years, a wide range of electrocatalytic materials have been developed for the H_2 evolution reaction (HER), but less research has been carried out on the development of materials for the water oxidation process.[18] To achieve successful green H_2 generation with minimal energy input, designing an efficient, low-cost, sustainable water oxidation catalyst is indispensable. Currently, existing water oxidation catalysts, such as RuO_2 and IrO_2, are known to be highly efficient, but their high costs and corrosive behaviour limit their industrial deployment.[19,20] Metal chalcogenides, particularly nickel chalcogenides, are receiving profound attention due to their catalytic activity for HER or oxygen evolution reactions (OER) in alkaline solutions.[21] However, enhancing the number of active sites remains a challenge for producing highly efficient HER and OER catalysts via a facile synthesis process.[22–24] Nickel selenides (NiSe) are the second largest studied nickel chalcogenides for electrocatalytic water splitting.[25,26] Four different types of nickel selenides are reported in the literature $Ni_{1-x}Se$ (0 < x < 0.15), $NiSe_2$, Ni_3Se_4 and Ni_2Se_3.[27] In general, nickel selenides are black in colour and do not dissolve in water. The insolubility of nickel selenides in water is a crucial parameter that makes them perfect for electrocatalytic water splitting applications. Interestingly, there is no other solvent that is capable of dissolving nickel selenides, but they tend to dissolve readily in highly oxidising acids, such as HNO_3.[27] Owing to its stability in neutral water and neutral water electrolyte solutions, NiSe is an appropriate catalyst for electrochemical water splitting in neutral and near-neutral media.

This study aims to explore the potential advantages of employing NiSe as a water oxidation electrocatalyst for the simultaneous generation of O_2 and H_2 gas from distillery industry wastewater. Several important factors were investigated in this research, including the stability of the NiSe coating, the performance of the catalyst over an extended period of time, and the overall stability of the materials before and after the electrolysis process. To assess the effectiveness of NiSe in the distillery wastewater electrolyte, all the obtained results are compared with those obtained in a freshwater (i.e., NaOH-based) electrolyte. This comparison provided a comprehensive evaluation of the performance and suitability of NiSe as an oxidative electrocatalyst to enhance H_2 generation from distillery wastewater.

2 Experimental

2.1 Chemicals

Selenium powder (Se, 99% purity); sodium tetrahydridoborate/sodium borohydride ($NaBH_4$, ≥99.8%); ethanol; sodium hydroxide; N,N-dimethylformamide (N,N-DMF, ≥99.8%); nickel(II) chloride hexahydrate ($NiCl_2 \cdot 6H_2O$) and ruthenium(IV) oxide (RuO_2, 99.9% purity) and dimethyl sulfoxide (DMSO, ≥99.9%) were purchased from Sigma-Aldrich. Deuterated water (D_2O) was purchased from Fisher Chemical. All chemicals were used without further purification. Milli Q water (18 ΩM) was used throughout the study.

2.2 NiSe catalysts preparation

The NiSe catalysts was prepared using solvothermal method. Typically, 0.32 g of Se powder was dispersed in 0.19 g of $NaBH_4$ before adding 30 mL of N,N-DMF. The resultant solution (solution A) was then mixed using a magnetic stirrer (200 rpm) for 1 h. After that, 0.48 g of $NiCl_2$ was added to solution A and placed back on the stirrer for a further stirring (200 rpm, 1 h), forming solution B. Once the desired time has elapsed, solution B was transferred to an autoclave jar (100 mL capacity) and kept in an electric furnace (Thermo Scientific) at 170 °C for a select duration of time. The electric furnace was switched off after completion of the desired time duration. The autoclave jar was left to cool to room temperature, after which the solution was transferred to a glass beaker. It was then washed with ethanol and water alternatively four times. During the washing process, the powder was collected using a centrifuge. The final powder sample was further annealed at 60 °C for 24 h in a vacuum drying oven. On completion of this process, the resultant NiSe nanomaterial was kept under vacuum conditions to prevent oxidation occurring in the material.

2.3 NiSe electrode fabrication

Briefly, 4.5 mg of the synthesized NiSe powder was dispersed in 3 mL ethanol and placed in an ultrasonic bath for 30 min. A stainless-steel substrate (316 L) was then placed on a hotplate at 100 °C. The NiSe ink was then removed from the ultrasonic bath and 100 μL was then immediately dispersed onto both sides of the substrate using a micropipette. After heating for a further 5 min, the electrode was suitably ready to carry required electrochemical experiments. The ultimate catalyst loading of NiSe on stainless steel is approximately 1.67 mg cm^{-2}.

2.4 Material characterisation

We conducted X-ray diffraction (XRD) analysis to delve into the crystalline structure of the NiSe powder (Malvern Panalytical Empyrean Diffractometer) equipped with Cu Kα radiation (l = 1.5418 Å) and compared with the ICDD-JCPDS powder diffraction file database. For a comprehensive understanding of its surface characteristics, we employed both field emission scanning electron microscopy (FE-SEM, Quanta 200 F FEI) and high resolution transmission electron microscopy (HRTEM, FEI Titan Themis 200) equipped with an energy-dispersive X-ray spectroscopy (EDX) detector operated at 200 kV. To gain

insights into the chemical composition and bonding states of NiSe, we employed X-ray photoelectron spectroscopy (XPS) (Kratos Axis Supra). Carbon 1s (284.6 eV) was used to calibrate the binding energies of other element scanned at high resolution. The distillery water was analysed with nuclear magnetic resonance spectroscopy (NMR, Bruker AVIII-400). Typically, 100 μL of the liquid sample was mixed with 100 μL of DMSO standard solution and 400 μL of D_2O in an NMR tube. The DMSO standard solution was made by diluting the DMSO with D_2O to obtain the final concentration (1.262 mM). The samples were analysed using ^1H NMR equipped with water suppression.

2.5 Electrochemical measurements

The electrochemical performance of NiSe was carried out using an electrochemical station (Autolab PGSTAT 302N), utilising the potentiostat function to apply the potential voltage to the system. NOVA software (version 2.1.5) was used to run the measurements for all experiments. The cell consisted of a typical 3 electrode system with a NiSe working electrode, Ni foam counter electrode and Hg/HgO (model: CHI 152, CH Instruments) reference electrode. A Hg/HgO reference electrode was selected as a suitable accompaniment to the 1.0 M NaOH (pH = 14.0) aqueous electrolyte that was used for all measurements. Polarisation curves were obtained from linear sweep voltammetry (LSV) studies in a potential range of −0.2 to 1.2 V vs. Hg/HgO. All measured potentials vs. the Hg/HgO were converted to the reversible H_2 electrode (RHE) scale via the Nernst equation:[28]

$$E_{vs.\ RHE} = E_{vs.\ Hg/HgO} + 0.098 + 0.059 \text{pH} \qquad (1)$$

where E_{RHE} is the converted potential vs. RHE. $E_{Hg/HgO}$ is the experimentally measured potential against the Hg/HgO reference electrode, and $E^{\circ}_{Hg/HgO}$ is the standard potential of Hg/HgO at 25 °C. The electrode surface area was kept constant at 3 cm² for all measurements.

The electrochemically active surface area (ECSA) of the Ni_2Se_3 coating on SS was determined based on cyclic voltammetry (CV) measurements. Various scan rates ranging from 0.001 V s⁻¹ to 0.1 V s⁻¹ at non-faradaic region potential were applied. The peak current was recorded for each scan rate and plotted against the current density.

2.6 Distillery wastewater

The distillery wastewater was collected by industrial partner the Scotch Whisky Research Institute. It contains trace amounts of alcohol, dissolved copper, caustic soda, etc. The distillery wastewater contained solid waste and was primarily removed by centrifuging at 10 000 rpm for 10 min. NaOH was added to the resultant solution to prepare 1.0 M of NaOH-distillery waste solution, which was used as the electrolyte for all electrochemical experiments.

2.7 H_2 generation

The H_2 generation from the electrochemical cells was measured using a gas chromatograph (GC, Agilent Technologies 7890B

equipped with TCD-FID detectors). The two-compartment electrochemical cell separated by a membrane (Nafion) was setup to measure H_2 evolution when a constant potential of 0.75 V vs. Hg/HgO was applied to the circuit. SS or Ni_2Se_3/SS and Ni foam were used as the electrodes and aqueous NaOH and NaOH-distillery wastewater were filled as the electrolyte in the anode and cathode compartments, respectively. The electrochemical compartments were sealed with a rubber stopper, which had an inlet and outlet port, to ensure minimal gas leakage. To push the generated H_2 into the GC, the inlet port on the cathode compartment was bubbled with N_2 (BOC, 99.995%, 0.8 mL min⁻¹) throughout the experiment. The outlet of the cathode compartment was connected to the GC sampling port for continuous injection of sample. Area under the curve obtained in each injection was used to quantify the amount of H_2 generated.

3 Results and discussion

The crystallinity of as-synthesized NiSe powder was characterised using XRD (Fig. 1a). The predominant XRD peaks exhibits at 29.9°, 33.5°, 33.57°, 42.9°, 50.7°, 55.5° and 57.5° confirmed the formation of cubic phase of Ni_2Se_3 (JCPDS – 1-1495).[29] When the Ni_2Se_3 powder was coated onto the SS, the XRD pattern did not show any significant difference when compared to the pristine Ni_2Se_3 powder (Fig. 1a). The morphology of Ni_2Se_3 were analysed using SEM and HRTEM. The hydrothermally synthesised Ni_2Se_3 revealed a highly dispersed spherical shape (∼30–50 nm of diameter), as shown in the SEM images (Fig. S1†). In addition, the Ni_2Se_3 nanoparticles exhibited an interconnected network (Fig. S1†), highlighting the possibility of good electrocatalytic performance due to its highly exposed and active catalytic surface area, and the catalyst's ability to promote electrolyte accessibility and accelerate electron transport.[30] The HRTEM image (Fig. 1b) clearly evidenced that the Ni_2Se_3 nanoparticles exhibit a size distribution ranging between 30–50 nm, which aligned with SEM results. Crystal plane of (111) with a d-spacing of 3.4 Å is indexed in Fig. 1c evidencing that the as-synthesized Ni_2Se_3 was highly crystallized. The elemental mapping analysis of the Ni_2Se_3 nanoparticle (Fig. 1d) revealed a uniform distribution of Ni and Se throughout the entire particle (Fig. 1e and f). The presence of oxygen (Fig. 1f) in the NiSe sample could potentially be attributed to atmospheric oxidation during sample characterisation or storage. It is important to consider the possibility of oxygen incorporation and its effects when interpreting the results and discussing the properties of the NiSe nanoparticles.

The chemical environment of the as-synthesised Ni_2Se_3 powder was analysed with XPS. The full-scan spectrum of $NiSe_2$ (Fig. 2a) confirmed the presence of Ni, Se, C, and O. The high-resolution of Ni 2p (Fig. 2b) shows that the characteristic peaks at 852.3 and 869.3 eV were attributed to Ni^{2+}, and the peaks located at 854.4 and 872.3 eV were originated from Ni^{3+}.[31–33] The Ni^{3+} most likely originated from the surface oxide phase. In addition, the broad peaks centred at 859.5 and 878.9 eV could be assigned to the satellite peaks (labelled as sat. in Fig. 2b). The Se 2d spectra displayed the characteristic peaks
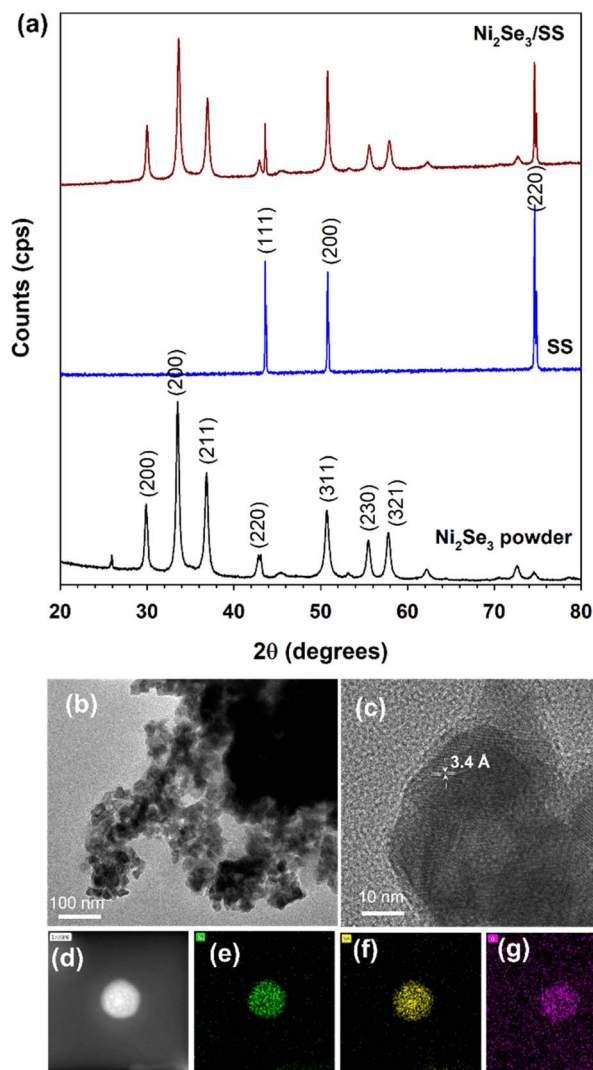
Fig. 1 (a) XRD pattern of Ni_2Se_3 powder, stainless steel substrate (SS) and Ni_2Se_3 coated SS (Ni_2Se_3/SS). HRTEM images of Ni_2Se_3 powder (b) at 100 nm scale and (c) 10 nm scale. (d) Elemental mapping of Ni_2Se_3 uniformly dispersing the elements of (e) Ni, (f) Se and (g) O.

Fig. 2 (a) High resolution of Ni 2p, (b) Se 3d, and (c) O 1s spectra of XPS using the as-synthesized Ni_2Se_3 powder sample.

at 54.5 eV and 55.1 eV which correspond to Se $3d_{5/2}$ and Se $3d_{3/2}$, respectively, indicated the existence of Se^{2-} (Fig. 2b).

Meanwhile, the broad peak located at 57.8 eV confirmed the oxidation state of Se.[34,35] The peak at 531.8 eV (Fig. 2c) was attributed to the oxygen of metal oxides, which may have resulted from the surface oxidising after exposure to air.[36]

The electrocatalytic activity of the Ni_2Se_3 anode was analysed in two different electrolytes, namely fresh water (NaOH solution only) and distillery wastewater (distillery wastewater and NaOH). To compare the performance, J–V plots obtained from linear sweep voltammetry of SS and Ni_2Se_3/SS electrodes in the presence of different anolyte were studied. During the process of water splitting for O_2 generation, an applied potential is employed in the cell. This potential initiates the oxidation of water molecules on the anode, resulting in the production of O_2.

Simultaneously, the by-product protons (H^+) are transported to the cathode surface through the membrane. At the cathode,
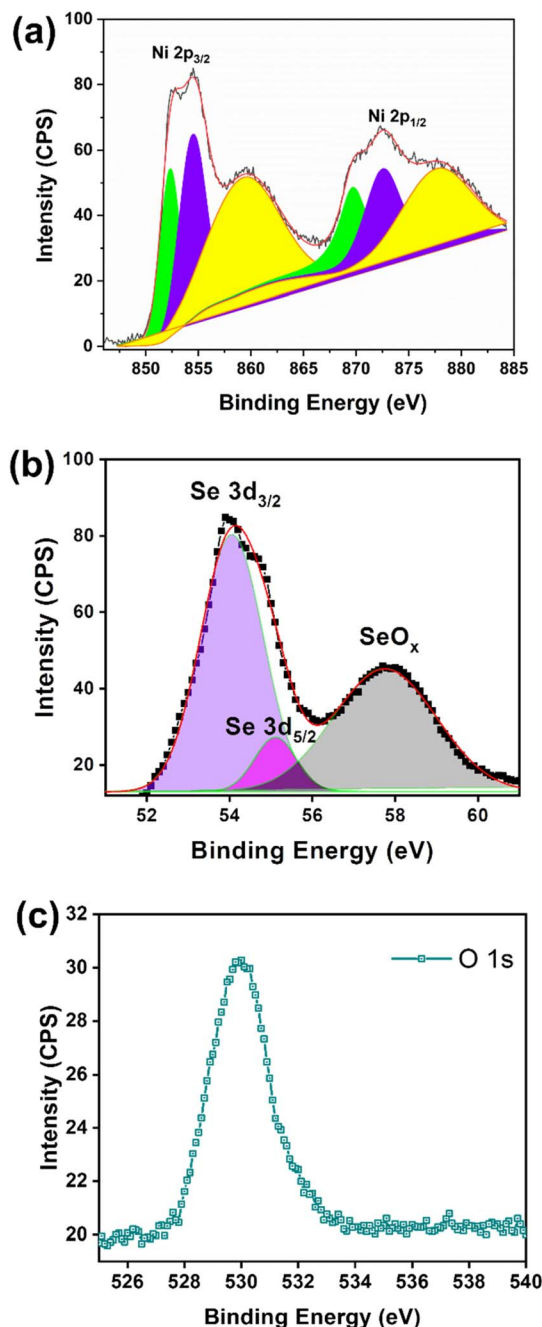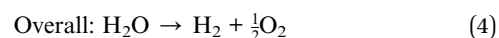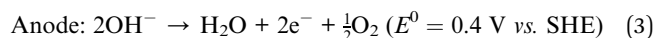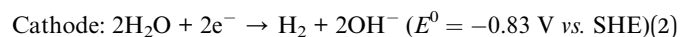
the protons undergo reduction and combine with electrons supplied by the circuit, generating H_2. The water splitting reactions occurring at the anode and cathode (alkaline environment) can be explained by the following reactions (eqn (2)–(4)):[37,38]

$$\text{Cathode: } 2H_2O + 2e^- \rightarrow H_2 + 2OH^- \ (E^0 = -0.83 \text{ V } vs. \text{ SHE}) \quad (2)$$

$$\text{Anode: } 2OH^- \rightarrow H_2O + 2e^- + \tfrac{1}{2}O_2 \ (E^0 = 0.4 \text{ V } vs. \text{ SHE}) \quad (3)$$

$$\text{Overall: } H_2O \rightarrow H_2 + \tfrac{1}{2}O_2 \quad (4)$$

These reactions elucidate the fundamental processes taking place during water electrolysis, in which the electrocatalytic activity of Ni_2Se_3 was crucial in enhancing the efficiency of these reactions. The current density generated by electrochemical cells indicate the electrocatalytic efficiency of the catalysts in O_2 and H_2 evolutions through OER and HER reactions (eqn (1) and (2)), respectively. Notably, the Ni_2Se_3/SS electrode (Fig. 3) exhibits a significantly higher current density of 223 mA cm^{-2} compared to the pristine SS electrode (146 mA cm^{-2}) in freshwater-based electrolyte, evidencing Ni_2Se_3 possessed superior OER activity. In particular, the Ni_2Se_3 catalyst reduced the overpotential of the pristine SS electrode from approximately 410 mV (@10 mA cm^{-2}) to 240 mV (@10 mA cm^{-2}), effectively demonstrating its efficacy in facilitating water oxidation reactions. Furthermore, the current density of Ni_2Se_3 experiences a notable improvement of ~21%, reaching 282 mA cm^{-2} at 2.1 V RHE in distillery industry wastewater, compared to the freshwater-based electrolyte (223 mA cm^{-2} at 2.1 V RHE). The increase in current density was attributed to the presence of organic moieties in the distillery wastewater that was evidenced using nuclear magnetic resonance (NMR) analysis (ESI Fig. S2a†). The current enhancement in distillery wastewater electrolyte was further examined by conducting cyclic voltammetry (CV) in the potential region between 0.9–1.9 V vs. RHE (Fig. 3b). Subsequently, we compare the CV results of Ni_2Se_3/SS anode using both freshwater and distillery wastewater electrolytes (Fig. 4).

A strong oxidation peak around 1.5 V RHE in the distillery wastewater-based electrolyte, which was absent in the freshwater electrolyte, was observed. This peak was attributed to the presence of acetate species in the distillery wastewater, which underwent an anodic oxidation reaction. It was proposed that when in contact with the electrocatalyst, acetate undergoes oxidation, generating oxidative electrons that significantly contribute to H_2 production by enhancing the rate of proton reduction at the cathode:[39]

$$2CH_3COO^- \rightarrow 2CO_2 + C_2H_6 + 2e^- \tag{5}$$

$$\text{At the cathode: } 2H^+ + 2e^- \rightarrow H_2 \tag{6}$$
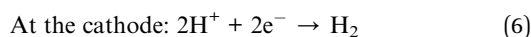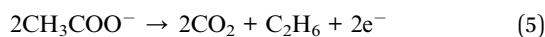
An alternative route for acetic acid oxidation, where acetic acid oxidation yields $8e^-$ (eqn (7))[40] and these oxidative electrons transfer to the cathode via the external circuit, which effectively reduces the protons under alkaline conditions, contributing to H_2 generation (eqn (6)).

$$CH_3COO^- + 6OH^- \rightarrow 2CH_4 + 4O_2 + H^+ + 8e^- \tag{7}$$

The proton diffusion coefficient (D_n) of distillery wastewater was estimated using CV plots at different scan rates (Fig. S4†) and determined using the following relation (eqn (8)).

$$I_p = 2.69 \times 10^5 \times n^{3/2} \times A \times D^{1/2} \times C \times \nu^{1/2} \tag{8}$$

where I_p is a peak current (amperes), "n" number of electrons transferred in a redox cycle, "A" the electrode surface area (cm^2), "C" molar concentration of redox-active species $(mol\ cm^{-3})$, "D"
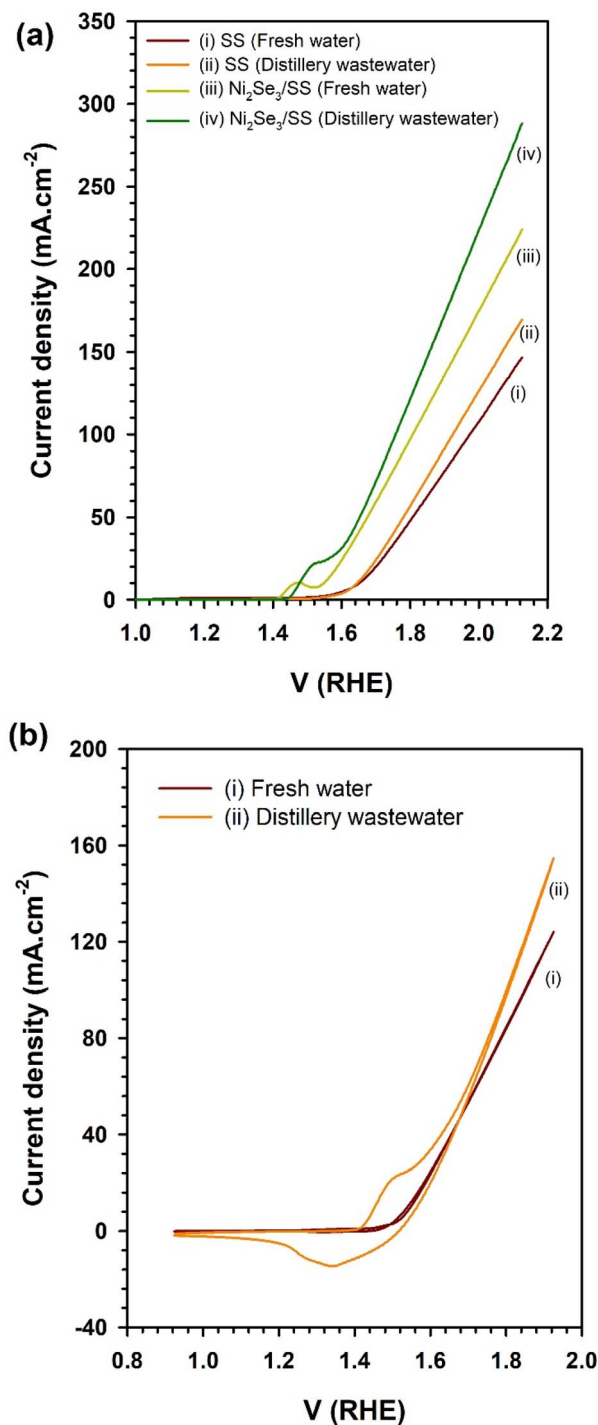

Fig. 3 (a) Linear sweep voltammogram results of stainless steel and Ni_2Se_3 nanoparticles coated stainless steel substates in freshwater and distillery wastewater electrolyte. (b) CV of Ni_2Se_3/SS anode in freshwater and distillery wastewater-based electrolyte. Note that the concentration of the electrolyte was 1 M NaOH.

the diffusion coefficient $(cm^2\ s^{-1})$ and "ν" scan rate in V s^{-1}. The estimated D_n value of distillery wastewater was found to be 2.28 $\times 10^{-9}\ cm^2\ s^{-1}$.

To compare the water oxidation performance of Ni_2Se_3 in with the commercial RuO_2, we conducted LSV tests (as
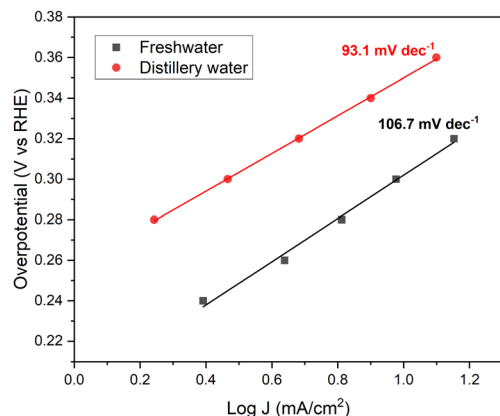
Fig. 4 Tafel plots of Ni_2Se_3 in freshwater and distillery wastewater electrolytes.

illustrated in Fig. S4†) under identical alkaline conditions, using a freshwater-based electrolyte. The current density of Ni_2Se_3 (Fig. S4†) reveals that it was comparable, particularly at higher applied potentials around 2 V RHE, when compared to the commercial RuO_2 catalyst. It's worth mentioning that RuO_2 is not the most ideal water oxidation candidate for demonstrating in alkaline electrolysis, as indicated by the Pourbaix diagram.[41]

The concentration of organic species (acetic acid) within the water significantly influences the overall performance of hydrogen generation during water splitting.[42,43] To investigate this effect, LSV tests were conducted using a Ni_2Se_3/SS anode in three distinct distillery water electrolytes: DW1, DW2, and DW3. These samples were collected at different stages of the water treatment process at the distillery industry site. The LSV results for DW1, DW2, and DW3 are presented in Fig. S5.† The data clearly indicates variations in current density across the distillery wastewater samples. This disparity in the current density was attributed to differences in the concentration of organic matter and the presence of heavy metals, such as copper, in the wastewater. Hence, the critical factor determining H_2 generation performance was the specific stage at which the samples were collected at the distillery water treatment site.

Tafel analysis is an invaluable tool that provides insights into both the activity and kinetics of electrochemical reactions simultaneously.[44,45] By plotting $\log J$ vs. V overpotential (RHE) (Fig. 4), the Tafel slope offers valuable information about the catalyst's self-oxidation and double-layer charging effects.[46] Additionally, Tafel slope data allows one to determine the required increase in overpotential to enhance the reaction rate by a factor of ten. In the case of Ni_2Se_3, the Tafel slope (Fig. 4) was estimated through chronoamperometry experiments. Notably, in distillery wastewater electrolyte, the Tafel slope of Ni_2Se_3 is significantly reduced to 93.1 mV dec^{-1}, compared to the freshwater-based electrolyte (106.7 mV dec^{-1}). This reduction suggests an improved performance of Ni_2Se_3 as an oxygen evolution reaction (OER) catalyst when operating in distillery wastewater. Furthermore, when compared to the conventional

OER catalyst PtC (120 mV dec^{-1}) in literature, the lower Tafel slope value of synthesised Ni_2Se_3 nanoparticles in the current work implies the potential of catalyst quality.[47] Nonetheless, when comparing the Tafel slope values of Ni_2Se_3 with those reported in previous literature, it becomes evident that there is room for further enhancement in the quality of Ni_2Se_3. This improvement can be achieved through various approaches, including careful substrate selection, innovative doping techniques, and the meticulous design of nanostructures. These strategies, as discussed in references, offer avenues for optimizing the performance and efficiency of Ni_2Se_3 catalysts.[48–53] A recent review conducted by Anantharaj et al.[54] has presented a comprehensive comparison of Tafel slope values of nickel selenide in electrochemical water oxidation reactions. Their findings revealed that Tafel values fall within the range of 24 to 128 mV dec^{-1} across various nanostructures, substrates, and electrolyte conditions. These results demonstrated the influence of different electrolyte compositions on the Tafel slope values of Ni_2Se_3 catalyst, emphasising the importance of considering the electrolyte conditions for optimizing the catalyst's performance in specific applications.

Electrochemical Impedance Spectroscopy (EIS) is a valuable tool for gaining insights into charge transfer resistance at electrode/electrolyte interfaces involved in electrochemical reactions.[55,56] It offers a means to understand the various components contributing to resistance, such as the catalyst,[57] electrolyte,[58] and membrane,[59] and how they collectively impact overall water splitting performance. In our current study, we employ EIS to investigate the reasons behind the superior current density achieved with distillery wastewater-based electrolytes in comparison to freshwater-based electrolytes. The EIS measurement was presented in Nyquist plots (Fig. 5) from the electrochemical cells featuring Ni_2Se_3/SS anodes and Ni foam cathode with different electrolytes. The impedance
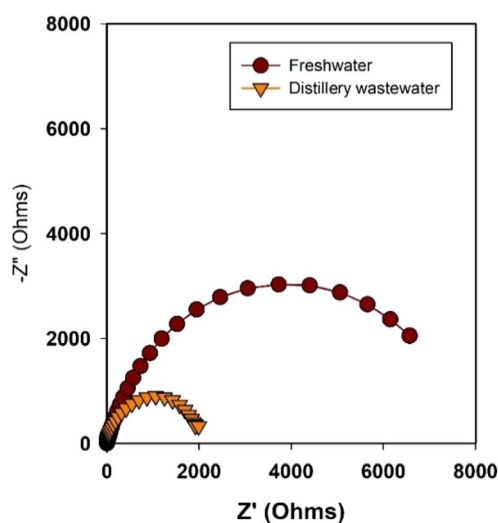

Fig. 5 Nyquist plots of Ni_2Se_3 (anode) and Ni mesh (cathode) in both freshwater and distillery wastewater electrolytes. It is important to note that impedance measurements were conducted at open circuit potential.

measurements were conducted at the open circuit potential (OCP), a state in which the catalyst's effect does not significantly impact the overall resistance of the cells. The diameter of the semicircles depicted in Fig. 5 corresponds to the charge transfer resistance values of the electrode/electrolyte interfaces. A wider semicircle signifies higher resistance, whereas a narrower one indicates lower resistance. In this context, the distillery wastewater-based electrolysis exhibited notably lower charge transfer resistance than its freshwater counterpart. This phenomenon was attributed to the presence of organic substances and potentially copper particles in the distillery wastewater, both of which contribute to lowering the overall electrolyte resistance. The lower electrolyte resistance is one of the reasons for the enhanced electrochemical performance in distillery water-based electrolytes.

The recovery of H_2 generation from wastewater pollutants treatment is an innovative approach in recent times. Notably, a wastewater electrolysis cell opens pathways for decentralised H_2 production with simultaneous on-site wastewater treatment.[60,61] The current density and corresponding H_2 production exhibited from the electrochemical cell with a Ni_2Se_3 anode is presented in Fig. 6. Though Ni_2Se_3 has shown higher current density in distillery wastewater-based electrolyte, an aggressive bubbling effect was observed at the cathode over time (see the Video in ESI†), This had the effect of reducing the catalytic activity of the Ni cathode in the production of H_2. As a result, the cell using freshwater electrolyte produced 0.37 mL min^{-1}; whereas distillery wastewater-based cell resulted in 0.25 mL min^{-1}. Overall, Ni_2Se_3 coated SS electrode was capable to produce ~13 mL h^{-1} cm^{-2} of H_2 from distillery wastewater. In the case of O_2 evolution at anode compartment, we observed distillery waste-based electrolyte produces higher oxygen evolution than fresh water based electrolyte (Fig. S6†). This is most likely due to the reduction of acetate (CH_3COO^-), which was formed after mixing NaOH into the distillery waste solution that contains notable amounts acetic acid, forming CH_4 and O_2 as illustrated in eqn (3). As a result, distillery wastewater produced three times the amount of CH_4 than that of

freshwater, and a continuous evolution of O_2 throughout the electrocatalytic measurement, which could be observed in the NMR (0.23 ppm in ^1H NMR) and GC (Fig. S2B†), respectively.

To assess the stability of the Ni_2Se_3/SS electrode in water oxidation reactions, a chronopotentiometry experiment was conducted at a current density of 10 mA cm^{-2}. Fig. S7† illustrates that the cell potential remained notably stable around 1.6 V RHE for a duration of 12 hours. This observation suggests that the Ni_2Se_3/SS electrode exhibited high stability when it exposed in distillery wastewater-based electrolyte. Following the completion of the 12 h chronoamperometry studies, we conducted a surface examination of the Ni_2Se_3/SS anode under SEM (Fig. S8a and b†). The SEM images reveal a slight increase in the size of the Ni_2Se_3 nanoparticles after the electrochemical reaction. This phenomenon was attributed to two factors: (a) the formation of a thin oxidation layer, SeO_2, during the reactions. (b) The agglomeration effect on the particles. Notably, despite these changes, there was no significant accumulation of particulate matter on the surface of the Ni_2Se_3 catalyst before or after the reaction. This observation underscored the significant surface stability of Ni_2Se_3 against electrochemical corrosion reactions, particularly in its ability to oxidise the organic substances present in the distillery wastewater (Fig. 3).

For a comprehensive assessment of catalytic performance and scalability potential, it is more informative to focus on a key metric: the turnover frequency (TOF). This metric quantifies the rate at which molecules (such as H_2 and O_2 in the context of water splitting) are produced per second per active site while maintaining a specific overpotential. In the present work, this approach is crucial for comparing the intrinsic catalytic activity of Ni_2Se_3 in freshwater and distillery water. As a pivotal measure in catalysis, the TOF per active Ni_2Se_3 site under freshwater and distillery water was computed for the OER, assuming 100% faradaic efficiency, and is presented in the accompanying Fig. 7. The TOF of oxygen generation using Ni_2Se_3/SS anode can be estimated using the relation:[62,63]

$$\text{TOF} = [\text{total oxygen turnovers (cm}^{-2})/\text{active sites density}] \quad (9)$$

$$\text{Active sites density} = (\text{number of active sites} \times \text{ECSA}) \quad (10)$$

A detailed estimation of total oxygen turnovers can be found in ESI.† ECSA calculations were performed using the following equation:

$$\text{ECSA} = (C_{DL})/C_s \quad (11)$$

Here, C_{DL} represents the electrochemical measurement of double-layer capacitance, obtained through differential capacitance measurements in a narrow potential region at different scan rates. The slope of the peak current against the scan rate in the non-faradaic region provides the C_{DL} value (Fig. S9a and b†). The specific capacitance (C_s) is a constant value dependent on the material and the electrolyte solution (alkaline or acidic). For this experiment, the C_s value for NiSe was held constant at 40 µF cm^{-2} adopted from the previous report.[64] The calculated ECSA
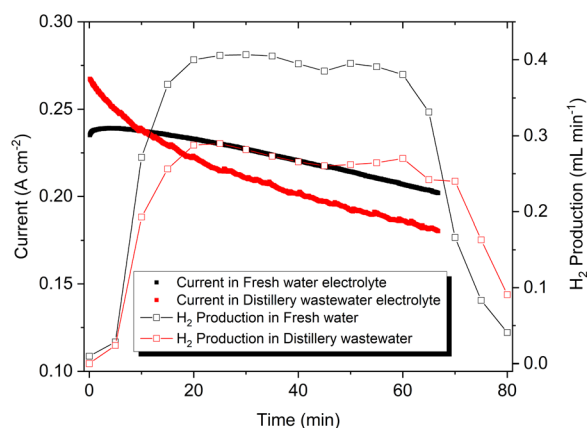

Fig. 6 H_2 generation of Ni_2Se_3/SS electrodes using fresh water (black) and distillery wastewater based electrolyte (red). Note that the concentration of electrolytes was 1.0 M NaOH.
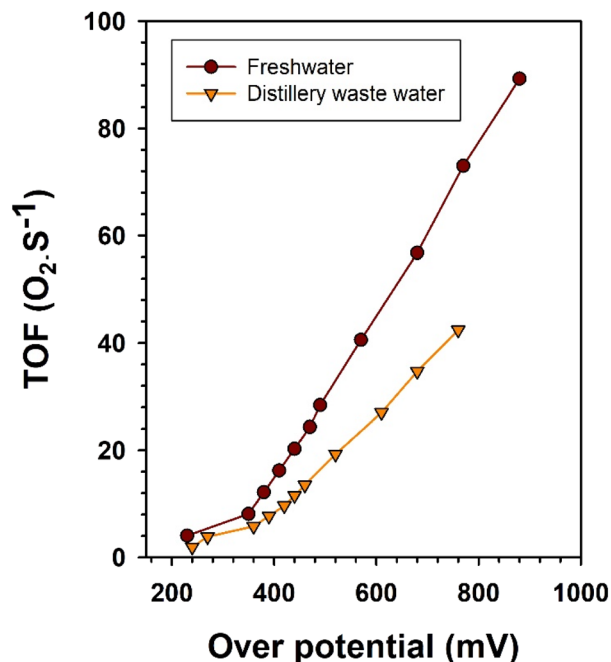
Fig. 7 TOF of Ni_2Se_3/SS anode in electrolytic oxygen generation performance in fresh water and distillery wastewater.

for Ni_2Se_3/SS is determined to be 11 cm^2 and 23.5 cm^2, for fresh water and distillery water based electrolyte, respectively. The TOF values of Ni_2Se_3/SS anode in freshwater and distillery wastewater is presented in Fig. 7.

Ni_2Se_3/SS anode exhibited a significantly higher TOF in freshwater when compared to distillery wastewater (Fig. 7). This observation suggested that Ni_2Se_3 has a notable capacity to catalyse the electrochemical oxidation of water molecules for oxygen generation at its active sites. In contrast, the lower TOF observed in distillery wastewater suggested a reduced capacity for oxygen generation. This could be attributed to the presence of competitive catalytic activities that favoured the oxidation of organic molecules, hampering the electrochemical water oxidation process.

We have comparatively analysed the electrocatalytic performance of Ni_2Se_3 synthesized in this study with recent reports on nickel selenide-based anodes, which were synthesized through different techniques, used in water splitting reactions (Table 1).

Notably, the Ni_2Se_3, which was synthesized *via* the solvothermal method, exhibited a significantly lower overpotential of 240 mV compared to other counterparts.

It is worth to note that when handling distillery wastewater, several considerations should be considered. Firstly, it is important to note that freshly collected distillery water samples tend to yield higher H_2 production due to the potential presence of alcohol molecules, which may evaporate into the atmosphere. To mitigate this, one of the recommended practices is to store the distillery samples at freezing temperatures to preserve the alcohol content. Additionally, conducting experiments involving varied temperatures can provide valuable insights into the impact of temperature on current density enhancement. Exploring the effects of temperature variations in electrochemical experiments could help to uncover the potential strategies for optimising H_2 production. Additionally, it is crucial to further test this electrolyte in a flow cell type setup. Such testing would help address critical issues related to electrolyte evaporation and any other associated challenges that may arise in practical applications. Flow cell configurations allow for continuous operation and can provide insights into the long-term stability and performance of the electrolyte, helping to assess its feasibility for scalable sustainable H_2 production from distillery wastewater. Furthermore, analysing the distillery wastewater after electrolysis can provide valuable information regarding the recovery of value-added products. Although this aspect is beyond the scope of the present study, investigating the potential recovery of valuable substances from the electrolyzed wastewater could be a worthwhile avenue for future research. Moreover, it is worth mentioning that the electrochemical activity of the NiSe nanoscale catalyst can be further improved through various approaches. These approaches can include modifying the coating method on steel substrates and exploring the use of highly conducting substrates as alternatives to steel.

To mitigate the bubbling effect at the cathode, effective approaches involve the incorporation of ultrasonic treatment[73] or cavitation treatment[74] at the cathode. For instance, a study conducted by Ehrnst and colleagues[73] showcased an enhancement in the HER performance. This improvement stems from the intense local electromechanical coupling induced by acoustic forcing. This acoustic influence disrupts the tetrahedrally-coordinated hydrogen bond network of water molecules at the electrode–electrolyte interface. Consequently,

Table 1 Comparative performance of the present study and other reports on nickel selenide anodes in water splitting reactions

Catalyst	Synthesis technique	Coating surface	Reference electrode	Electrolyte	Overpotential (mV) measured @ 10 mA cm^{-2}	References
NiSe$_2$	Chemical vapour deposition	Glassy carbon	Ag/AgCl	1 M KOH	230	65
NiSe/NiO$_x$	Solvothermal	Ni foam	Hg/HgO	1 M KOH	243	66
NiSe	Electrodeposition	Au coated glass	Hg/HgO	1 M KOH	290	67
NiSe$_2$	Solvothermal	Glassy carbon	Ag/AgCl	1 M KOH	378	68
NiSe$_2$/MoSe$_2$	Hydrothermal/selenization	Glassy carbon	Hg/HgO	1 M KOH	295	69
NiSe$_2$/NiO nanosheet	Selenization	Glassy carbon	Hg/HgO	1 M KOH	300	70
NiSe-2	Electrodeposition	Ni foam	SCE	1 M KOH	252	71
NiSe@Ni	Electrodeposition/selenization	Stainless steel	Ag/AgCl	1 M KOH	290	72
Ni$_2$Se$_3$	Solvothermal	Stainless steel	Hg/HgO	1 M NaOH	240	Present work

it leads to the generation of a higher concentration of "free" water molecules, making them more accessible to catalytic sites on the unmodified polycrystalline electrode. By optimizing these factors, the performance and efficiency of the NiSe catalyst can be enhanced for future applications.

4 Conclusions

In conclusion, our study successfully synthesised nanoscale Ni_2Se_3 catalysts through a solvothermal method and evaluated their performance as water oxidation catalysts in electrolysis H_2 generation, using both freshwater and distillery industry wastewater. Notably, the nano scale Ni_2Se_3 catalyst coated on a SS electrode exhibited a significantly higher current density in distillery industry wastewater-based electrolytes compared to NaOH. At an applied potential of 0.75 V Hg/HgO, it demonstrated the production of approximately 13 mL h^{-1} of H_2, with a relatively stable performance. However, it is essential to acknowledge the challenges posed by the presence of bubbles on the anode and cathode surfaces, resulting from biomass oxidation and reduction processes. These bubbles have a significant impact on sustainable H_2 generation. To address this issue, the implementation of bubble removal techniques (ultrasonic treatment, cavitation), in conjunction with the electrolyser, show a promising and forward-thinking approach to safeguard the electrode surface and ensure long-term sustainability. Furthermore, future research endeavours could focus on conducting additional experiments to analyse the by-products generated after the electrolytic oxidation of distillery wastewater. Such investigations would provide valuable insights into the pathways of the oxidation process at the anode. This work contributes to the advancement of utilizing biomass industry wastewater as a feedstock for the electrolysis process, thereby reducing the extensive freshwater footprint associated with green H_2 generation. Our findings underscore the potential of harnessing alternative and sustainable resources in the pursuit of clean and eco-friendly energy solutions.

Author contributions

SP conceived the idea, acquired funding, and wrote, reviewed and edited the manuscript. MW performed materials synthesis, electrochemical and analytical experiments and drafted the manuscript. JZYT demonstrated the materials characterisation, product analysis and gas quantification analysis and writing. SN, JA, and helped with the data analysis and proofreading.

Conflicts of interest

There are no conflicts to declare.

Acknowledgements

References

1 F. P. Colelli, J. Emmerling, G. Marangoni, M. N. Mistry and E. D. Cian, *Nat. Commun.*, 2022, **13**, 4964.

2 B. J. van Ruijven, E. D. Cian and I. S. Wing, *Nat. Commun.*, 2019, **10**, 2762.

3 J. A. Turner, *Science*, 2004, **305**, 972–974.

4 J. Jia, L. C. Seitz, J. D. Benck, Y. Huo, Y. Chen, J. W. D. Ng, T. Bilir, J. S. Harris and T. F. Jaramillo, *Nat. Commun.*, 2016, 7, 13237.

5 M. Wang, Z. Wang, X. Gong and Z. Guo, *Renewable Sustainable Energy Rev.*, 2014, **29**, 573–588.

6 S. G. Simoes, J. Catarino, A. Picado, T. F. Lopes, S. di Berardino, F. Amorim, F. Gírio, C. M. Rangel and T. Ponce de Leão, *J. Cleaner Prod.*, 2021, **315**, 128124.

7 S. Pitchaimuthu, K. Sridharan, S. Nagarajan, S. Ananthraj, P. Robertson, M. F. Kuehnel, Á. Irabien and M. Maroto-Valer, *Energies*, 2022, **15**, 7399.

8 R. R. Beswick, A. M. Oliveira and Y. Yan, *ACS Energy Lett.*, 2021, **6**, 3167–3169.

9 Y. Chen, *Nat. Rev. Earth Environ.*, 2022, **3**, 604.

10 K. R. Davies, M. G. Allan, S. Nagarajan, R. Townsend, V. Asokan, T. Watson, A. R. Godfrey, M. M. Maroto-Valer, M. F. Kuehnel and S. Pitchaimuthu, *Ind. Eng. Chem. Res.*, 2023, **62**, 19084–19094.

11 K. R. Davies, M. G. Allan, S. Nagarajan, R. Townsend, T. Dunlop, J. D. McGettrick, V. S. Asokan, S. Ananthraj, T. Watson, A. R. Godfrey, J. R. Durrant, M. M. Maroto-Valer, M. F. Kuehnel and S. Pitchaimuthu, *J. Environ. Chem. Eng.*, 2023, **11**, 110256.

12 K. Cho, D. Kwon and M. R. Hoffmann, *RSC Adv.*, 2014, **4**, 4596–4608.

13 B. Jones, K. R. Davies, M. G. Allan, S. Anantharaj, I. Mabbett, T. Watson, J. R. Durrant, M. F. Kuehnel and S. Pitchaimuthu, *Sustainable Energy Fuels*, 2021, **5**, 3084–3091.

14 C. Edwards, C. C. McNerney, L. A. Lawton, J. Palmer, K. Macgregor, F. Jack, P. Cockburn, A. Plummer, A. Lovegrove and A. Wood, *Resour., Conserv. Recycl.*, 2022, **179**, 106114.

15 J. S. White, K. L. Stewart, D. L. Maskell, A. Diallo, J. E. Traub-Modinger and N. A. Willoughby, *ACS Omega*, 2020, **5**, 6429–6440.

16 R. Price, L. MacDonald, N. Gillies, A. Day, E. Brightman and J. Li, *Faraday Discuss.*, 2023, **247**, 270–290.

17 C. Duffy, D. Styles, I. Schestak, K. Macgregor, F. Jack, D. Henn, K. Black and P. P. M. Iannetta, *J. Cleaner Prod.*, 2023, **395**, 136436.

18 B. M. Hunter, H. B. Gray and A. M. Müller, *Chem. Rev.*, 2016, **116**, 14120–14136.

19 F.-Y. Chen, Z.-Y. Wu, Z. Adler and H. Wang, *Joule*, 2021, **5**, 1704–1731.

20 Y. Wang, L. Zhang, K. Yin, J. Zhang, H. Gao, N. Liu, Z. Peng and Z. Zhang, *ACS Appl. Mater. Interfaces*, 2019, **11**, 39728–39736.

21 Y. Liu, Y. Guo, Y. Liu, Z. Wei, K. Wang and Z. Shi, *Energy Fuels*, 2023, **37**, 2608–2630.

22 H. Ren, Z.-H. Huang, Z. Yang, S. Tang, F. Kang and R. Lv, *J. Energy Chem.*, 2017, **26**, 1217–1222.

23 J. Yin, J. Jin, H. Lin, Z. Yin, J. Li, M. Lu, L. Guo, P. Xi, Y. Tang and C.-H. Yan, *Advanced Science*, 2020, **7**, 1903070.

24 Y. Wang, B. Yu, M. He, Z. Zhai, K. Yin, F. Kong and Z. Zhang, *Nano Res.*, 2022, **15**, 4820–4826.

25 A. T. Swesi, J. Masud, W. P. R. Liyanage, S. Umapathi, E. Bohannan, J. Medvedeva and M. Nath, *Sci. Rep.*, 2017, **7**, 2401.

26 J. Zhang, Y. Wang, C. Zhang, H. Gao, L. Lv, L. Han and Z. Zhang, *ACS Sustain. Chem. Eng.*, 2018, **6**, 2231–2239.

27 S. Anantharaj, S. Kundu and S. Noda, *J. Mater. Chem. A*, 2020, **8**, 4174–4192.

28 C. Wang, W. D. Wu, Y. Wang, D. Xu and F. Yan, *New J. Chem.*, 2017, **41**, S2.

29 Z. Zhuang, Q. Peng, J. Zhuang, X. Wang and Y. Li, *Chem.–Eur. J.*, 2006, **12**, 211–217.

30 R. Andaveh, A. Rouhaghdam, J. Ai, M. Maleki, K. Wang, A. Seif, G. B. Darband and J. Li, *Appl. Catal., B*, 2023, **325**, 122355.

31 Y. Zhang, Y. Liu, M. Ma, X. Ren, Z. Liu, G. Du, A. M. Asiri and X. Sun, *Chem. Commun.*, 2017, **53**, 11048–11051.

32 J. Yang, Z. Sun, J. Wang, J. Zhang, Y. Qin, J. You and L. Xu, *CrystEngComm*, 2019, **21**, 994–1000.

33 M. Zhu, Q. Yan, Y. Xue, Y. Yan, K. Zhu, K. Ye, J. Yan, D. Cao, H. Xie and G. Wang, *ACS Sustain. Chem. Eng.*, 2021, **10**, 279–287.

34 M. Zhu, D. Zhang, Q. Lu, Y. Yan, K. Zhu, K. Ye, J. Yan, D. Cao, Q. Wang, X. Huang and G. Wang, *Int. J. Hydrogen Energy*, 2021, **46**, 20524–20533.

35 J.-N. Huang, B. Wen, J.-G. Zhu, Y.-S. Zhang, J.-Z. Gao and Z.-Z. Chen, *Sci. Total Environ.*, 2020, **733**, 138929.

36 Y. Du, G. Cheng and W. Luo, *Catal. Sci. Technol.*, 2017, **7**, 4604–4608.

37 Y. Li, L. Zhou and S. Guo, *EnergyChem*, 2021, **3**, 100053.

38 C. Huang, J. Zhou, D. Duan, Q. Zhou, J. Wang, B. Peng, L. Yu and Y. Yu, *Chin. J. Catal.*, 2022, **43**, 2091–2110.

39 S. D. Ross, M. Finkelstein and R. C. Petersen, *J. Am. Chem. Soc.*, 1964, **86**, 4139–4143.

40 D. Karakashev, D. J. Batstone, E. Trably and I. Angelidaki, *Appl. Environ. Microbiol.*, 2006, **72**, 5138–5141.

41 K. Du, L. Zhang, J. Shan, J. Guo, J. Mao, C.-C. Yang, C.-H. Wang, Z. Hu and T. Ling, *Nat. Commun.*, 2022, **13**, 5448.

42 B. You, X. Liu, N. Jiang and Y. Sun, *J. Am. Chem. Soc.*, 2016, **138**, 13639–13646.

43 T. Kahlstorf, J. N. Hausmann, T. Sontheimer and P. W. Menezes, *Global chall.*, 2023, **7**, 2200242.

44 T. Shinagawa, A. T. Garcia-Esparza and K. Takanabe, *Sci. Rep.*, 2015, **5**, 13801.

45 R. Sanchis-Gual, A. Seijas-Da Silva, M. Coronado-Puchau, T. F. Otero, G. Abellán and E. Coronado, *Electrochim. Acta*, 2021, **388**, 138613.

46 S. Anantharaj, S. Noda, M. Driess and P. W. Menezes, *ACS Energy Lett.*, 2021, **6**, 1607–1611.

47 Y.-Y. Sun, M.-Y. Jiang, L.-K. Wu, G.-Y. Hou, Y.-P. Tang and M. Liu, *Sustainable Energy Fuels*, 2020, **4**, 582–588.

48 Z. Feng, L. Ren, Y. Liu and B. Gao, *J. Solid State Electrochem.*, 2023, **27**, 1469–1476.

49 S. Dutta, A. Indra, Y. Feng, T. Song and U. Paik, *ACS Appl. Mater. Interfaces*, 2017, **9**, 33766–33774.

50 C. Tang, N. Cheng, Z. Pu, W. Xing and X. Sun, *Angew. Chem., Int. Ed.*, 2015, **54**, 9351–9355.

51 O. A. Oyetade and R. J. Kriek, *Electrocatalysis*, 2020, **11**, 35–45.

52 C. An, Y. Wang, P. Jiao, S. Wu, L. Gao, C. Zhu, J. Li and N. Hu, *Catalysts*, 2022, **12**, 1055.

53 B. Singh and A. Indra, *Chem.–Asian J.*, 2020, **15**, 607–623.

54 S. Anantharaj and S. Noda, *Int. J. Hydrogen Energy*, 2020, **45**, 15763–15784.

55 S. Anantharaj and S. Noda, *ChemElectroChem*, 2020, **7**, 2297–2308.

56 S. Wang, J. Zhang, O. Gharbi, V. Vivier, M. Gao and M. E. Orazem, *Nat. Rev. Methods Primers*, 2021, **1**, 41.

57 A. R. C. Bredar, A. L. Chown, A. R. Burton and B. H. Farnum, *ACS Appl. Energy Mater.*, 2020, **3**, 66–98.

58 L. Zhu, P. Yang, W. Lyu, Q. Wang and K. Wang, *Int. J. Electrochem. Sci.*, 2022, **17**, 22099.

59 Y. Jing and B. P. Chaplin, *J. Membr. Sci.*, 2016, **511**, 238–249.

60 H. Park, C. D. Vecitis and M. R. Hoffmann, *J. Phys. Chem. C*, 2009, **113**, 7935–7945.

61 H. Park, C. D. Vecitis and M. R. Hoffmann, *J. Phys. Chem. A*, 2008, **112**, 7616–7626.

62 A. Karmakar and S. Kundu, *Mater. Today Energy*, 2023, **33**, 101259.

63 J. Kibsgaard and T. F. Jaramillo, *Angew. Chem., Int. Ed.*, 2014, **53**, 14433–14437.

64 R. Andaveh, A. S. Rouhaghdam, J. Ai, M. Maleki, K. Wang, A. Seif, G. B. Darband and J. Li, *Appl. Catal., B*, 2023, **325**, 122355.

65 I. H. Kwak, H. S. Im, D. M. Jang, Y. W. Kim, K. Park, Y. R. Lim, E. H. Cha and J. Park, *ACS Appl. Mater. Interfaces*, 2016, **8**, 5327–5334.

66 R. Gao, G.-D. Li, J. Hu, Y. Wu, X. Lian, D. Wang and X. Zou, *Catal. Sci. Technol.*, 2016, **6**, 8268–8275.

67 U. De Silva, J. See, W. P. R. Liyanage, J. Masud, J. Wu, W. Yang, W.-T. Chen, D. Prendergast and M. Nath, *Energy Fuels*, 2021, **35**, 4387–4403.

68 S. K. Ramesh, V. Ganesan and J. Kim, *ACS Appl. Energy Mater.*, 2021, **4**, 12998–13005.

69 C. Yin, F. Yang, S. Wang and L. Feng, *Chin. J. Catal.*, 2023, **51**, 225–236.

70 Z. Liu, C. Zhang, H. Liu and L. Feng, *Appl. Catal., B*, 2020, **276**, 119165.

71 Z. Feng, H. Zhang, L. Wang, B. Gao, P. Lu and P. Xing, *J. Electroanal. Chem.*, 2020, **876**, 114740.

72 Y.-Y. Sun, Y.-X. Zhu, L.-K. Wu, G.-Y. Hou, Y.-P. Tang, H.-Z. Cao and G.-Q. Zheng, *Electrochim. Acta*, 2020, **353**, 136519.

73 Y. Ehrnst, P. C. Sherrell, A. R. Rezk and L. Y. Yeo, *Adv. Energy Mater.*, 2023, **13**, 2203164.

74 A. Angulo, P. van der Linde, H. Gardeniers, M. Modestino and D. F. Rivas, *Joule*, 2020, **4**, 555–579.